# Modelling of the Transient Electric Field in Multilayer Dielectric Composites Under Impulsive HV Energization

Timothy Wong, *Graduate Student Member, IEEE, Igor Timoshkin, Senior Member, IEEE, Scott MacGregor, Senior Member, IEEE, Mark Wilson, Member, IEEE, Martin Given, Senior Member, IEEE*

***Abstract*— This article presents the theoretical analysis of composite electrical insulation, formed from layered dielectric materials and subjected to impulsive energization. One-dimensional planar and cylindrical geometries were considered, consisting of an arbitrary number of layers with arbitrary relative permittivity and electrical conductivity. Analytical solutions have been succesfully derived for the time-dependent electric field inside the i-th layer. To demonstrate the usage of the model under complex multilayer topologies where analytical solutions are non-trivial, the characteristics of a 20–layer graded composite under microsecond and sub-microsecond impulses were analyzed and validated against a finite-element solver. Results indicate that the transient electric field response under impulsive energization is strongly dependent on the interplay between the composite relaxation time constants and the characteristic timescales associated with the applied impulse. The model is a further development for the design and coordination of functionally graded materials (FGMs) and composite insulation for high voltage system design. This is particularly relevant under fast-rising impulsive conditions as often encountered in many pulsed power applications.**

***Index Terms*— multilayer dielectric, functionally graded materials (FGM), analytical solution, high voltage, composite insulation, pulsed power systems**

## I. Introduction

IN high voltage power and pulsed-power equipment, the presence of fast-rising impulsive voltages can impose a significant degree of transient electrical stress on system components, which often presents a unique and difficult challenge for insulation design. Failure to account for peak field enhancement at critical regions such as triple-junctions may lead to insulation failure and electrical breakdown. In recent years, there has been increased research interest in novel field grading methods, motivated by the ever-increasing complexity of HV systems, the drive towards system miniaturization, and the development of novel pulsed power technology. Examples include various geometrical modifications to existing system accessories, the use of surface grading through conductive coatings [1], [2], or the use of field-adaptive grading materials [3]–[6].

Promising developments are functionally graded (FGMs) and composite materials, which employ spatially non-uniform distributions of permittivity and/or electrical conductivity as a means of field grading. It is remarked that conventional field-grading materials designed with field-adaptive characteristics may also be referred to as FGMs, e.g., [3]–[6], but the focus of this study is on materials with spatially nonuniform properties. Both continuous [7] and layered FGMs [8] have been described in the literature, where the former typically provides a smoother field distribution, but with significant manufacturing complexity and at higher cost when compared to the latter. However, in recent times, progress has been made toward more effective fabrication techniques for FGMs, e.g., centrifugal methods using particulate fillers [9], fused-deposition modelling (FDM) [10], the flexible mixture casting (FMC) method [11], or injection-based techniques [12], among several others. Indeed, each method has its own strengths, drawbacks, and optimisation techniques which will not be described in detail within this study. For this, the reader is referred to [9]–[13], and references therein.

A number of published studies have successfully demonstrated the application of FGMs to high voltage systems, with the majority focused on gas insulated system (GIS) spacers for AC or HVDC power transmission applications. An earlier paper by Hayashi *et al.* [14] reported on the breakdown behaviour of layered composites with a relative permittivity range of $\varepsilon_r$ = 3.0–5.9 under AC and lightning impulses, comparing their dielectric performance to those of homogeneous samples with $\varepsilon_r$ = 5.9. Experimental results revealed around 10%–25% increase in the breakdown voltage associated with the flashover of graded spacers under positive lightning impulses. The improvement observed from the layered FGM can be explained by the field grading effect, i.e., redistribution of the field across the gas-spacer interface. Using a disk-type spacer topology between plane-plane electrodes, simulations presented in [14] showed 23% and 44% reduction

Manuscript received Month XX, 2022; revised Month YY, 2022.

The authors are with The Department of Electronic and Electrical Engineering, High Voltage Technology Research Group, University of Strathclyde, Glasgow, U.K., G1 1XQ. (e-mail: timothy.wong@strath.ac.uk). 

in tangential field strength for spacers following inverse and inverse-square grading profiles, respectively.

Kurimoto *et al.* [15] demonstrated FGMs with a 'U' shape permittivity profile for radially graded cone-type GIS spacers. Modelled results indicated 38%–63% and 51%–62% field reduction near the anode and cathode triple-junctions, respectively. The authors describe the fabrication of the spacer using an epoxy resin matrix with $TiO_2$ and $Al_2O_3$ microparticles as fillers, and estimations presented in [15] suggest that FGMs may also possess superior operational lifetime over uniform materials.

Other studies conducted during a similar period include work by Ju *et al.* [16], [17] who presented an optimization methodology for the design of GIS spacers using a novel elliptical grading profile, predicting approximately 26% reduction of the maximum field strength. More recent studies by Hayakawa *et al.* [9], [18] present a manufacturing technique for radially-graded GIS spacers using a centrifugal method. An analytical model was also developed and validated against experimental data, which was able to predict the resultant permittivity distribution of the FGM. In [11], a further casting method is shown for axially graded spacers using $SiTiO_3$ and $SiO_2$ filler microparticles in epoxy resin - the authors analytically predict up to 70% increase in discharge inception voltage in $SF_6$ at reduced pressures. Computational studies were subsequently conducted by Imai *et al.* [12], [19], which overall demonstrated that resin distributions resulting from the casting method could be reasonably predicted from simulation.

Du *et al.* [20] combined a traditional volume-graded FGM spacer with surface flourination, reporting up to 36% higher DC flashover strength. Zhang *et al.* [21] investigated the application of novel carbon nanotube doped SiR material for power cable joints, where multilayer and pointwise FGMs were studied under AC and DC energization and found that FGM joints can substantially improve field uniformity. Talaat *et al.* [22] performed a computational study on FGM cone-type spacers using radially graded multilayer composites in the presence of a conducting particle. Their findings suggest that the application of certain FGMs may reduce the susceptibility of spacer interfaces to local field enhancement around contaminant particles. A detailed computational model was developed by Rachmawati *et al.* [7], who studied the influence of various permittivity and conductivity profiles on GIS spacers. In their work, the temperature and field dependence of conductivity was also modelled under DC steady-state, DC polarity reversal, DC-on (which incorporates a transition from zero to full applied voltage), and DC steady-state superimposed with lighting impulse conditions. The authors conclude that a 'U' shaped permittivity profile, combined with a conductivity distribution which only increases near the ground electrode, was, overall, the most effective at reducing the maximum field at the triple-junction.

Multilayer composites under impulsive regimes, however, have been studied to a far lesser extent. Under transient conditions, both the permittivity and electrical conductivity of each composite layer play a crucial role in determining the performance and characteristics of the insulating system. Modern pulsed power systems often utilise fast-rising impulses

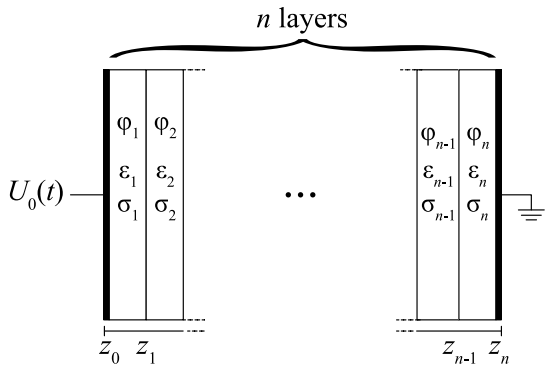


Fig. 1. Diagram of one-dimensional *n*-layer poorly-conducting composite energized between parallel plane electrodes.

with rise times in the range of hundreds of picoseconds to microseconds [23], and have found applications across many areas of engineering. Some examples include high-speed switching technology [24], pulsed electric field (PEF) treatment for biomedical and food processing industries [25], [26], to pollution control [27] and defence applications [28]. Therefore, there is an increased interest to characterise novel insulation solutions under fast transient signals and in non-standard topologies, as it has become critical for the optimisation and further development of these technologies. However, there exist few scenarios where fast transient stresses can be treated in the same way as steady state AC or DC, therefore necessitating a fully transient approach to the analysis.

In the present study, a theoretical approach for analyzing the transient electric field inside multilayered composites is presented. An analytical model has been developed for the estimation of the electric field developed inside an $n$-layer, poorly-conducting composite under fast-rising impulses. The motivation to employ an analytical approach is to have the ability to gain far deeper insights into the underlying physical behaviour compared to computational modelling. It additionally allows for the rapid estimation of the relevant design parameters, far faster than the use of conventional FE analysis and at minimal computational cost, facilitating parametric and optimisation studies. Using this model, the transient field characteristics have been analyzed, and the capability of the model is further demonstrated in the context of FGMs for GIS spacers.

## II. Mathematical Model

### A. Model Geometry and Governing Equations

A one-dimensional planar configuration was initially considered in this work, comprised of $n$ layers of poorly-conducting material (i.e., material which is characterized by its relative permittivity and electrical conductivity), stacked between parallel-plane electrodes. A cross-section of this layered structure is shown in Fig. 1. Each layer indexed $i$ is defined by a constant relative permittivity, $\varepsilon_i$, electrical conductivity $\sigma_i$ in S/m, and thickness $h = (z_i - z_{i-1})$ in meters, where $z_i$ is the $z$ coordinate of the boundary between the $i$-th and $(i+1)$-th layers. As the primary purpose of the present study is for fast-rising pulsed conditions, the temperature dependence of

conductivity was neglected, as there would be no significant change in temperature over such short timescales. It is also well-known that conductivity exhibits a highly nonlinear dependence upon the electric field, such that its inclusion would almost certainly render an analytical solution impossible. This dependence has, therefore, been omitted from the present work and constant conductivity is assumed. However, it should be noted that there exist two important cases for which this assumption is valid: (i) under sufficiently low-field or (ii) fast-rising voltage conditions. The first pertains to the far weaker dependence of $\sigma(E)$ for common insulating materials below an approximate value of $10^6 - 10^7$ V/m, see, for instance, [29]. The second assumes that the conductivity requires time to rise, as investigated in some materials in [30], [31], and that the relaxation time of the conduction process [30] is far longer than the rise time of the applied impulse. Under either one of these conditions, the conductivity can reasonably be assumed to exhibit minimal change with the field. It should further be noted that even if it were possible to incorporate $\sigma(E)$ dependence into the model using existing expressions found in the literature, these are typically derived under steady-state conditions, and their validity under fast transient conditions remains to be fully established. For boundary conditions, it was assumed that the stack would be energized through an arbitrary time-varying voltage $U_0(t)$ applied to the high voltage electrode, whilst the ground electrode is held at zero volts.

The potential field developed in the stack, assuming negligible space-charge effects, will be governed by Laplace's equation which in the present one-dimensional case reads:

$$\frac{d\varphi_i(z,t)}{dz^2} = 0, \tag{1}$$

where $\varphi_i(z,t)$ is the spatially and temporally varying electric potential in the $i$-th layer with units of volts. Equation (1) has the general solution:

$$\varphi_i(z,t) = A_i(t)z + B_i(t), \tag{2}$$

where $A_i(t)$ and $B_i(t)$ are time-dependent coefficients unique to each layer. The corresponding electric field $\mathbf{E}_i(t)$ is computed from the gradient of the potential, from which one finds:

$$\mathbf{E}_i(t) = -A_i(t)\hat{\mathbf{z}}. \tag{3}$$

### B. Boundary Conditions

At the electrodes, the ground potential at $z = 0$ and applied potential $U_0(t)$ at $z = z_n$ must be prescribed. Additionally, at each interface between two adjacent layers, the potential must be continuous across the boundary. These potential conditions take the form of (4)–(6):

$$\varphi_1(z = 0, t) = U_0(t), \tag{4}$$
$$\varphi_n(z = z_n, t) = 0, \tag{5}$$
$$\varphi_i(z = z_i, t) = \varphi_{i+1}(z = z_i, t). \tag{6}$$

Furthermore, the current continuity condition of (7) must be applied across each interface, stipulating that the sum of the conduction and displacement currents at each side of a layer boundary must be equal. This condition additionally takes into account the accumulation of unbound surface charge due to the Maxwell-Wagner effect,

$$\sigma_i E_i(z_i,t) + \varepsilon_0\varepsilon_i \frac{dE_i(z_i,t)}{dt} = \sigma_{i+1}E_{i+1}(z_i,t) + \varepsilon_0\varepsilon_{i+1}\frac{dE_{i+1}(z_i,t)}{dt}. \tag{7}$$

## III. Analytical Solutions

### A. Solution in the s-domain

The system formed by (1)–(7) can be converted to simple algebraic forms through the application of the Laplace transform, from which one can show that, in the Laplace $s$-domain,

$$B_{i-1}(s) = A_i(s)z_{i-1} - A_{i-1}(s)z_{i-1} + B_i(s), \tag{8}$$

which takes the form of a recursive addition from $i = 1$ to $i = n$, and can be expanded and rearranged to give

$$\begin{aligned} B_0(s) = {} & A_2(s)z_1 - A_1(s)z_1 + A_3(s)z_2 + A_4(s)z_3 \\ & - A_3(s)z_3 + A_5(s)z_4 - A_4(s)z_4 \ldots \\ & + A_n(s)z_{n-1} - A_{n-1}(s)z_n + B_n(s). \end{aligned} \tag{9}$$

Following (4), it can be shown that $B_0(s) = U_0(s)$. As such, its substitution into (9) yields the expression

$$U_0(s) = \sum_{k=1}^{n} A_k(s)\left(z_{k-1} - z_k\right). \tag{10}$$

Rearranging the $s$-domain form of (7) provides a similar recursive relation between the $A$ coefficients of adjacent layers, ultimately allowing $A_i(s)$ to be expressed as

$$A_i(s) = \frac{U_0(s)}{\sigma_i\left(1+\tau_i s\right)}\left[\sum_{k=1}^{n}\frac{\left(z_{k-1}-z_k\right)}{\sigma_k\left(1+\tau_k s\right)}\right]^{-1}, \tag{11}$$

where $\tau_i$ is the intrinsic relaxation time constant for the $i$-th layer, defined as:

$$\tau_i = \frac{\varepsilon_0\varepsilon_i}{\sigma_i}. \tag{12}$$

### B. Existence of Closed-form Time-domain Solutions

To model the field distribution in different practical multi-layered systems, it would be convenient to obtain a closed-form time-domain solution for the field distribution. Analysis of the general $s$-domain solution (11) has been conducted and one can show that there exists an upper limit to $n$ for which a closed-form time-domain solution is possible. An expanded form of (11) can be written

$$A_i(s) = U_0(s)\frac{\prod_{j=1,j\neq i}^{n}\sigma_j\left(1+\tau_j s\right)}{\sum_{k=1}^{n}\left(\left(z_{k-1}-z_k\right)\prod_{j=1,j\neq k}^{n}\sigma_j\left(1+\tau_j s\right)\right)}, \tag{13}$$

where the denominator can be shown to be a polynomial in $s$ with degree $n-1$. This is to say,

$$\sum_{k=1}^{n}\left((z_{k-1}-z_k)\prod_{j=1,j\neq k}^{n}\sigma_j\left(1+\tau_j s\right)\right)\equiv a_0 s^{n-1}+a_1 s^{n-2}+a_2 s^{n-3}+\ldots \ldots+a_{n-2}s^1+a_{n-1}s^0, \tag{14}$$

where $a_0 \ldots a_n$ are constant coefficients that are strictly negative. As such, the factorization of the denominator must result in:

$$A_i(s)=U_0(s)\frac{\prod_{j=1,j\neq i}^{n}\sigma_j\left(1+\tau_j s\right)}{a_0\left(s+\frac{1}{\tau_{n+1}}\right)\left(s+\frac{1}{\tau_{n+2}}\right)\ldots\left(s+\frac{1}{\tau_{2n+1}}\right)} = \frac{U_0(s)}{a_0}\frac{\prod_{j=1,j\neq i}^{n}\sigma_j\left(1+\tau_j s\right)}{\prod_{m=1}^{n-1}\left(s+\frac{1}{\tau_{n+m}}\right)}, \tag{15}$$

where the additional $n-1$ time constants are derived from the roots of the scaled characteristic polynomial of the system,

$$P_n=s^{n-1}+\frac{a_1}{a_0}s^{n-2}+\frac{a_2}{a_0}s^{n-3}+\ldots+\frac{a_{n-1}}{a_0}s^0, \tag{16}$$

and hence:

$$\tau_{n+m}=-\frac{1}{\text{roots}(P_n)_m}. \tag{17}$$

Considering (16) and (17), the Abel-Ruffini theorem [32] states that the roots to a polynomial of degree $\geq 5$ with arbitrary coefficients cannot be expressed in radicals. Thus, one concludes that no closed-form solutions to (17) can be found for $n>5$. For $n=1$, (11) reduces to the elementary solution $U_0(s)/z_1$. For $n=2$, the degree of $P_n$ is 1, thus allowing (17) to be solved by simple rearrangement. For $n=3$ to 5, the roots can be found by means of the closed-form quadratic, cubic, and quartic formulas, respectively. If $n$ exceeds 5, a solution can be sought by solving (17) via any preferred numerical root-finding method, such as the application of the eigenvalue theorem which are available in popular symbolic math toolboxes. Examples with $n=20$ are presented from section IV onwards. Up to this point, it should be noted that the analysis has been conducted assuming an arbitrary $s$-domain voltage $U_0(s)$. The general solution (11) is therefore applicable to any applied waveform, so long as the the signal has an analytical $s$-domain form. For instance, sinusoidal AC, DC, exponential impulses, ramps, or superpositions of the above are all equally possible.

### C. Time-domain Solution For Impulsive Voltage

In this work, time-dependent impulsive voltages were of interest, which are applied to the high voltage electrode. The voltage waveform is analytically represented by the commonly used double-exponential form of (18):

$$U_0(t)=A_0U_0\left(e^{-\alpha t}-e^{-\beta t}\right), \tag{18}$$

where $U_0$ is the peak voltage magnitude in volts, $A_0$ is a dimensionless scaling parameter, while $\alpha$ and $\beta$ are wave-shaping parameters in $s^{-1}$, which control the rise (front) and fall (tail) characteristics of the impulse. Applying the Laplace transform to (18) and using (11) yields the $s$-domain double-exponential solution:

$$E_i(s)_{DE}=-\frac{A_0U_0}{a_0}\frac{(\beta-\alpha)\prod_{j=1,j\neq i}^{n}\sigma_j\left(1+\tau_j s\right)}{(s+\alpha)(s+\beta)\prod_{m=1}^{n-1}\left(s+\frac{1}{\tau_{n+m}}\right)}, \tag{19}$$

from which the inverse transform allows the derivation of the time-domain field magnitude inside any layer $i$:

$$E_i(t)_{DE}=-\frac{A_0U_0}{a_0}\left[\frac{P(\alpha)}{Q(\alpha)}e^{-\alpha t}-\frac{P(\beta)}{Q(\beta)}e^{-\beta t}+(\beta-\alpha)\sum_{m=1}^{n-1}\frac{R(m)}{S(m)}e^{-\frac{t}{\tau_{n+m}}}\right], \tag{20}$$

where:

$$P(x)=\prod_{j=1,j\neq i}^{n}\sigma_j\left(1-x\tau_j\right),\quad Q(x)=\prod_{m=1}^{n-1}\left(\frac{1}{\tau_{n+m}}-x\right),$$
$$R(x)=\prod_{j=1,j\neq i}^{n}\sigma_j\left(1-\frac{\tau_j}{\tau_{n+x}}\right),$$
$$S(x)=\left(\alpha-\frac{1}{\tau_{n+x}}\right)\left(\beta-\frac{1}{\tau_{n+x}}\right)\prod_{\substack{k=1\\k\neq x}}^{n-1}\left(\frac{1}{\tau_{n+k}}-\frac{1}{\tau_{n+x}}\right). \tag{21}$$

The coefficients given by (21) together with the roots from (16) show that the transient response of the electric field in any layer is determined by the complex interplay between the relaxation characteristics of every other layer present in the composite, and of the transient characteristics of the applied impulse. This aspect is analysed in further detail from section IV onwards.

### D. Extension to the Cylindrical Domain

Cylindrical conductors with concentric insulation layers are of significant practical importance to power and pulsed power systems. Examples include cables with conductors wrapped in multiple layers of insulation, or gas insulated switchgear (GIS) spacers, which may be graded in the radial direction. It can

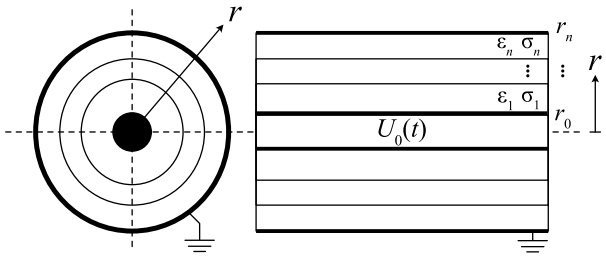


Fig. 2. Diagram of concentric cylindrical *n*-layer poorly-conducting composite, with the innermost boundary energized by a HV signal, and the outermost layer being held at ground potential.

be shown that with minimal changes to (11), the model can be extended to a cylindrical domain.

Consider a cylinder of radius $r$ as shown in Fig. 2, from which we may approximate the geometry using 2D polar coordinates. If the inner conductor of radius $r_0$ is wrapped in $n$ layers of material, then the radius of the $i$-th layer is denoted as $r_i$. It is further assumed that the outer layer at $r = r_n$ is grounded. The general solution of the Laplace equation in the radially symmetric polar domain takes the form:

$$\varphi_i(r,t) = C_i(t)\ln r + D_i(t), \tag{22}$$

where $C_i(t)$ and $D_i(t)$ are once again time-dependent coefficients unique to each concentric layer, synonymous to the previously used $A_i$ and $B_i$, but renamed to avoid overlap. The boundary conditions (4)–(7) once again apply, with the exception that $z$ is replaced with $r$, and $U_0(t)$ occurs at some $r = r_0$ rather than $r = 0$. The intermediate steps are identical to those of (8)–(11), except with instances of $(z_{k-1} - z_k)$ replaced with $\ln r_{k-1} - \ln r_k$. Equations (17) onward remain unchanged, as the differences in geometry are accounted for within the polynomial coefficients of (16). The radially decaying field magnitude in the $i$-th layer is then given by:

$$E_i(r,t) = -\frac{C_i(t)}{r}. \tag{23}$$

## IV. Grading Characteristics of Multilayered Composites Under Fast-Rising Impulses

In this section, the results arising from the application of the model to FGMs are presented. The analytical nature of the model, coupled with the inclusion of arbitrary permittivity and conductivity in each layer, allows for rapid parametric and optimization studies to be performed. Thus, the model has the potential to be used in the design of layered or composite insulation systems under generalized time-dependent stresses, including for pulsed applications. Subsections IV-A and IV-B follow to independently analyze the effects of permittivity and conductivity grading under fast-rising signals, respectively. Computational results gathered using a finite-element electrostatic solver package QuickField Professional version 6.4 [33] are also presented alongside the analytical model for validation. QuickField has the capability to conduct transient electric field analysis, allowing direct comparison of (20) to numerically simulated results. It should be noted

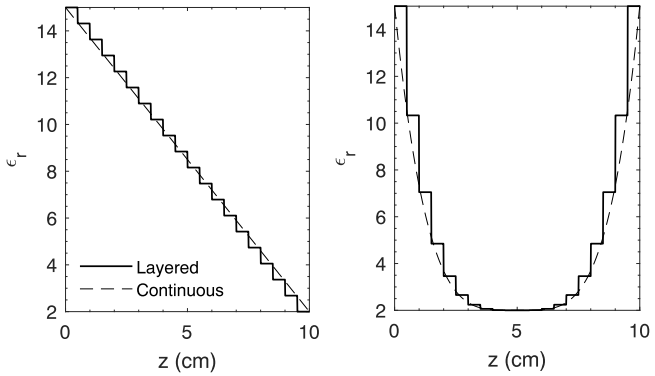


Fig. 3. Plot of the spatial variation of relative permittivity for a 20-layer composite with: (*left*) linearly-decreasing permittivity with distance, and (*right*) 'U'-shaped distribution, which is symmetrical about $z$ = 5 cm.

that due to the limitation of linearly-spaced finite timesteps in QuickField, data points shown in Fig. 6 and Fig. 8 become irregularly spaced on a logarithmic scale. Simulation results are therefore not shown after 1 $\mu$s to maintain the visibility of other plotted data, but have been confirmed to continue following the analytical solution. It is further remarked that while experimental validation would be invaluable to ascertain these effects in practise, the fabrication of layered composites and the accurate measurement of intra-layer fields under high speed impulses is nontrivial. An experimental investigation was therefore considered outside the scope of the present theoretical study, though it would be of high interest to conduct such an investigation in the future.

### A. Graded Permittivity

A 20-layer composite material was considered, with two different permittivity grading profiles under demonstration: (i) a linearly-decreasing profile, and (ii) a 'U'-shaped profile. Equations (24) and (25) have been developed to provide the parameter value at a given layer based upon the layer position, corresponding to the two profiles described above. Linear and quartic polynomials have been used to interpolate the parameter values for the two profiles, yielding:

$$p_i^{\text{linear}} = p_{\max} + \frac{p_{\max} - p_{\min}}{z_{n-1}} z_{i-1}, \tag{24}$$

$$p_i^{\text{U-shape}} = \frac{16\,(p_{\max} - p_{\min})}{z_{n-1-a}^4}\left(z_{i-1} - \frac{z_{n-1-a}}{2}\right)^4 + p_{\min}. \tag{25}$$

Here, $p_{\max}$ and $p_{\min}$ are the maximum and minimum desired parameter values (relative permittivity or electrical conductivity), and $a = (1-(-1)^n)/2$ is either 1 or 0 depending on the parity of $n$. If $n$ is even, (25) holds only up to $i = n/2$, after which the resultant values for $p$ must be reflected. Each layer in the composite is maintained at an equal thickness of $h$ = 0.25 cm to give a total inter-electrode gap of 5 cm. In the results presented in this section, the electrical conductivity of all layers was set to zero, such that the field relaxation in the bulk could be ignored, enabling the effects of permittivity grading to be isolated. The spatial variations of the relative permittivity for each of the aforementioned profiles are shown

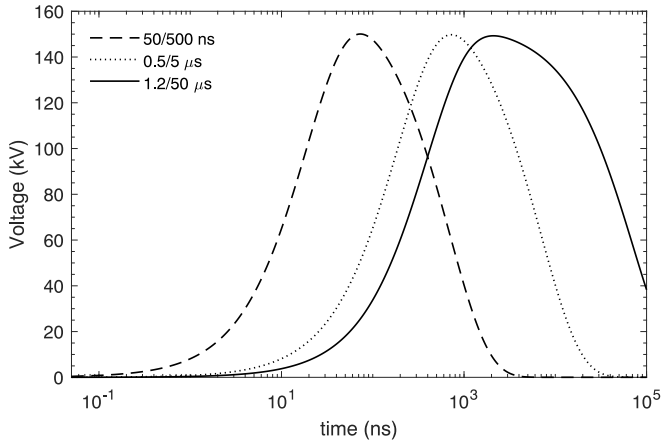


Fig. 4. The computed impulsive waveforms following the double-exponential definition of (18). Dashed line: 50/500 ns, dotted line: 0.5/5 $\mu$s, solid line: 1.2/50 $\mu$s.

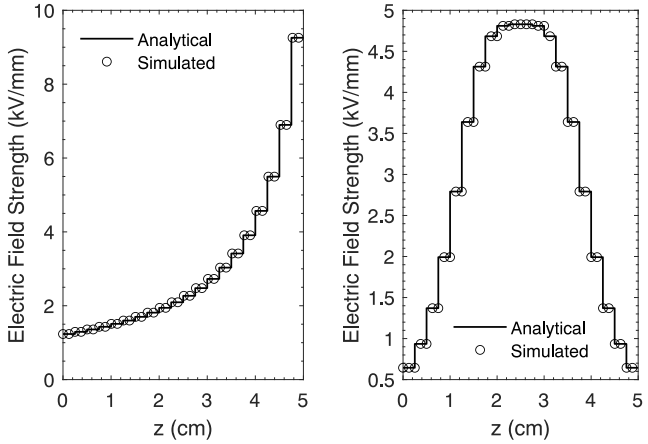


Fig. 5. Field distribution in the 20-layer composite under (*left*) the linear grading profile, and (*right*) the 'U'-shaped graing profile, under permittivity grading for the planar geometry. Data for the peak of applied 50/500 ns impulse, $t_p \sim 73.1$ ns. Analytical solution corresponds to (20), simulated data from QuickField.

in Fig. 3, using $\varepsilon_{\max} = 15$ and $\varepsilon_{\min} = 2$. The choice of these values is based upon relative permittivity values for common insulating materials, for example, polymeric materials, (cross-linked polyethylene (XLPE), polypropylene (PP), $\varepsilon_r = 2 \sim 3$, [34]), ceramics (Macor, Alumina, $\varepsilon_r = 6 \sim 9$ [35]), and an upper range ($\varepsilon_r = 12 \sim 15$) possibly attained by some composite grading materials [36].

Using a particle-swarm-like optimization algorithm, the double-exponential wave-shaping parameters emulating a 50/500 ns impulse voltage (50 ns front time and 500 ns time-to-half value) were calculated, giving $A_0 \sim 1.1454$, $\alpha \sim 144.8861 \times 10^4$ s$^{-1}$, and $\beta \sim 49.8516 \times 10^6$ s$^{-1}$. This impulse voltage is applied to the HV electrode with a peak voltage magnitude of 150 kV, the full waveform of which is included in Fig. 4 (dashed line). The two additional waveforms in this figure are used later, in section IV-C. The analytically-predicted field distribution developed inside the composite is shown with overlaid simulation results in Fig. 5, while the transient field responses in layers $i$ = 1, 5, 10, and 15 are

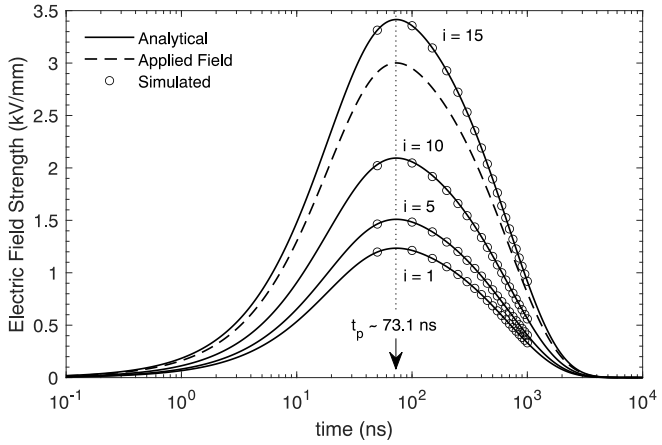


Fig. 6. Transient field response for the layers $i$ = 1, 5, 10, and 15 in the 20-later composite for the planar geometry using the linear (permittivity) grading profile. All layer conductivity values were set to 0 S/m. Analytical solution corresponds to (20), simulated data from QuickField.

included in Fig. 6. For the purposes of demonstration, only results from the planar geometry are presented in this section. The field response follows the same trends in a cylindrically symmetric case, with the main exception being the radial decay of the field.

Excellent agreement is found between the analytical predictions of (20) and the numerically simulated solution. For materials with zero conductivity, the electric field inside the composite layers behave as expected. Since there is no influence from conduction currents, the rise and fall characteristics of the electric field in each layer mimic those of the applied signal. The magnitude of the electric field strength in each case, however, is strongly determined by the relative permittivity of the corresponding layer, whereby the degree to which the field is reduced is positively correlated with its respective value of $\varepsilon_r$ due solely to polarisation. The field is therefore rejected from the high-permittivity layers toward the lower permittivity layers.

## B. Graded Conductivity

To investigate the influence of electrical conductivity grading, a complementary study was conducted for a $\sigma$ profile, but with identical $\varepsilon_r$ for all layers. In this case, the material with the highest electrical conductivity was placed adjacent to the electrodes, in regions where the field typically requires reduction. The relative permittivity in all layers was set equal to $\varepsilon_r = 2$, which reflects a typical value found for many polymeric insulators commonly used in engineering applications. The geometry and signal attributes remained the same as before, with the exception that now the electrical conductivity was graded following the profiles described by (24) and (25), with $\sigma_{\min} = 10^{-14}$ S/m (approximate range for common engineering polymers) and $\sigma_{\max} = 10^{-4}$ S/m (possible range attained by commercially-available conductive grading tapes [37]). Once again, the analytical field distributions and transient responses using the linear profile are shown in Fig. 7 and 8, along with the numerical solution computed from QuickField.

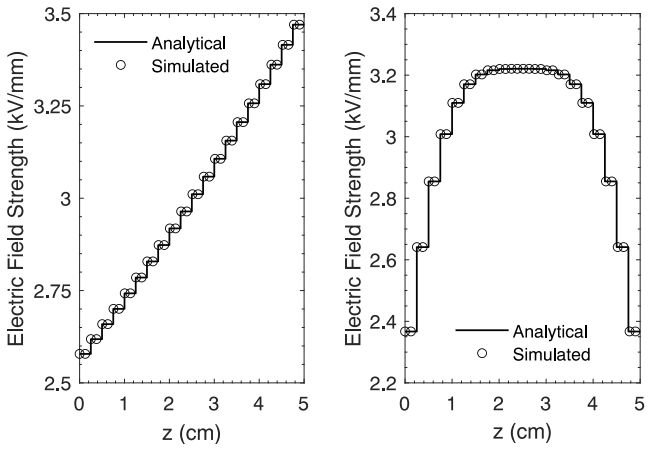


Fig. 7. Field distribution in the 20-layer composite under (*left* the linear grading profile, and (*right*) the 'U'-shaped grading profile, under conductivity grading for the planar geometry. Data for the peak of applied 50/500 ns impulse, $t_p \sim 73.1$ ns. Analytical solution corresponds to (20), simulated data from QuickField.

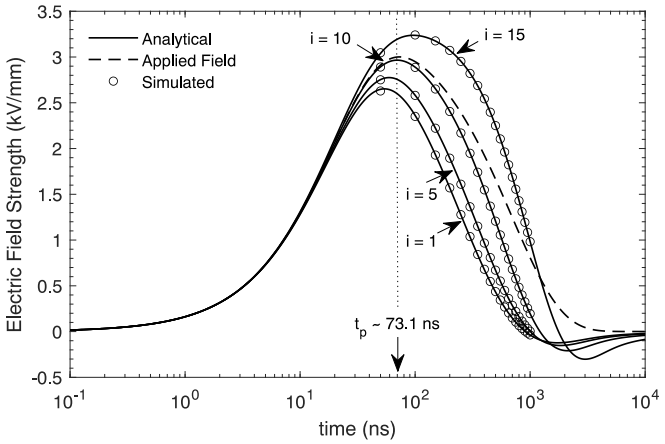


Fig. 8. Transient field response for the layers $i$ = 1, 5, 10, and 15 in the 20-layer composite for the planar geometry under the linear (conductivity) grading profile. All layer relative permittivity values were set to $\varepsilon_r$ = 2. Analytical solution corresponds to (20), simulated data from QuickField.

With non-zero electrical conductivity, the field relaxation characteristics of the various layers was shown to influence and modify the transient response of the composite. Both the peak magnitude of the electric field, and the peak time at which this maximum occurs in any layer, showed strong dependence upon the electrical conductivity in all other layers. Analytically, this behaviour follows from the $n-1$ additional time constants arising from the characteristic polynomial, and captures the complex relationship between the different relaxation times which govern the dynamics of interfacial surface charge accumulation due to the Maxwell-Wagner effect. Under the linear grading profile, the direction of the field was also observed to reverse near the wave-tail, at around $t = 1$ $\mu$s. This is believed to be the result of decaying surface charge at the interfaces between dielectric layers. The time required for the surface charge to dissipate at any interface was shown to be a complex function of the permittivity and conductivity distribution of the entire composite, which, in general, will not be equal for all layers. Therefore, on the falling edge of the impulse, the field in the $(i+1)$-th layer may momentarily be in the opposite direction to that of the $i$-th layer due to the differing rates of surface charge decay at the $i$-th layers' interfaces. The field then gradually decays back to zero as the levels of surface charge at all interfaces decay to zero. Under the present linear grading profile, the field in each layer therefore reverses polarity consecutively, starting from $i = 1$ up to $i = 20$ in sequential order.

### C. Effects of Wave Shape

Under combined permittivity and conductivity grading, the effects of the applied wave-shape on the transient field response of the composite were also studied in this work. A wide variety of pulse shapes are utilized across various pulsed power applications [23]–[28], which can range from picoseconds to microseconds in front time. As demonstrated in section IV-B, the presence of layers with non-zero conductivity can substantially modify the transient behaviour of the developed field inside the composite. Therefore, it is of great interest and high importance to characterize how a given composite would react under different impulses, particularly for applications which may be sensitive to the wave-shape, such as PEF treatment [25], [26]. In addition to the 50/500 ns signal previously characterized, we further introduce a 0.5/5 $\mu$s impulse, and a standard 1.2/50 $\mu$s lightning impulse according to IEC 60060 standards [38], as was shown in Fig. 4. These specifications were chosen to represent waveforms which are increasingly slower-rising than the original (50/500 ns) waveform. The peak voltage remained at 150 kV, and the corresponding wave-shaping parameters are tabulated in Table I.

The combined grading scheme follows that of the 'U' shaped profile for both relative permittivity and conductivity, with the same values as used in sections IV-A and IV-B. Fig. 9 plots the transient field responses for $i = 1$ and 10, corresponding to the positions where the field exhibits the most significant reduction and enhancement, based upon the choice of grading profile.

It should be noted that, due to the symmetry of the grading profile about the interface of the 10$^{\text{th}}$ and 11$^{\text{th}}$ layers, the field responses were found to be mirrored, such that $i = 1$, 20 or $i = 2$, 19 etc., have identical responses. Evidently, for all three impulsive wave-shapes, the fields at the electrodes are effectively reduced, each with a similar peak reduction of ~85%. The successful redistribution of the field to the middle of the composite material is also clear, however, the peak field magnitude which was developed differs significantly between the various applied waveforms. Around 10% higher

TABLE I
DOUBLE-EXPONENTIAL WAVE-SHAPING PARAMETERS FOR THE UTILIZED IMPULSIVE WAVEFORMS.

| Waveform Specification | $A_0$ | $\alpha$ (s$^{-1}$) | $\beta$ (s$^{-1}$) |
|---|---|---|---|
| 50/500 ns | 1.1454 | $144.8861\times10^4$ | $49.8516\times10^6$ |
| 0.5/5 $\mu$s | 1.1418 | $144.7250\times10^3$ | $50.2967\times10^5$ |
| 1.2/50 $\mu$s | 1.0305 | $13.9621\times10^3$ | $24.8658\times10^5$ |

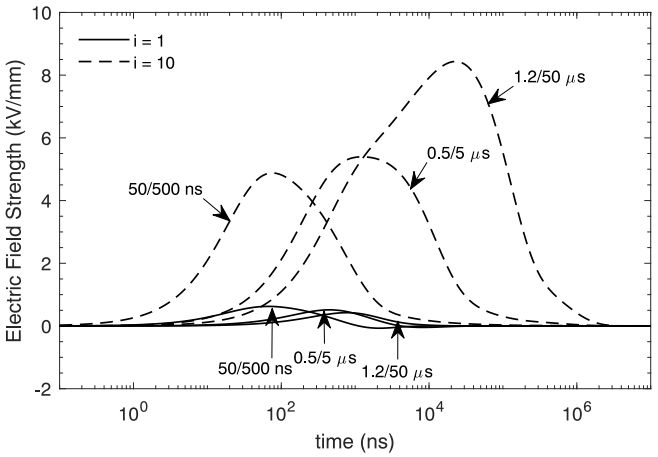


Fig. 9. Transient field response for the layers $i$ = 1 and 10 in the 20-layer composite under combined permittivity and conductivity grading, following the 'U'-profile and under energization by the three waveforms described in Fig, 4 and Table I.

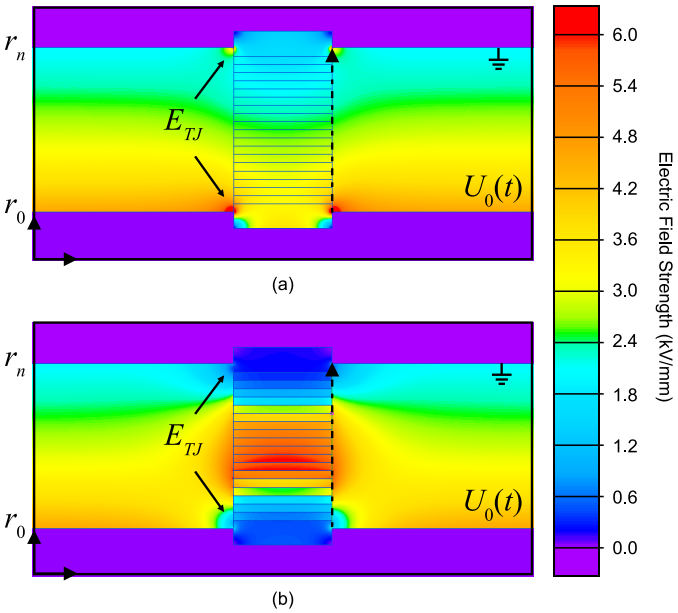


Fig. 10. Field distribution near disk-type GIL spacer for (a) uniform spacer material, and (b) $\varepsilon$ and $\sigma$ graded material following 'U' profile. Images were taken when the field enhancement at the interface was at its maximum. Dashed contour depicts path of measurement for Fig. 11 (on the side of the gas).

peak field is estimated for the 0.5/5 $\mu$s signal compared to 50/500 ns, while a substantial difference of around 40% is exhibited for the 1.2/50 $\mu$s impulse. The likely cause of such wide variation are the magnitudes of the composite relaxation times relative to the applied impulse time constants. For the system studied here, system time constants arising from the characteristic polynomial range from a maximum of around 23 ms to a minimum of around 1.3 $\mu$s, with most of them existing between 1-10 $\mu$s. For fast input signals with short front-times (e.g., 50/500 ns), the inability for the system to react to the rapidly changing external field results in a reduced maximum at the center of the composite, as there is insufficient time for the field to be excluded fully from the outer layers. This is consistent with Fig. 9, which shows a higher peak field in layer 1 for faster signals. To the contrary, when the input front-time is similar to or longer than the above range (e.g., 1.2/50 $\mu$s), the dielectric layers are able to respond to a greater extent and redistribute the field inward on a similar timescale to that required for the applied field to peak. Therefore, a much higher degree of peak field enhancement at the center, and stronger field reduction at the electrodes, are observed. It follows therefore that this effect would likely have the greatest impact when the relaxation times of the composite are significantly longer than that of the characteristic timescales of the applied impulse.

It has therefore been shown that the grading effectiveness of a layered composite under impulsive stress strongly depends upon the transient characteristic of the applied signal and of the composite itself. Consequently, for the purposes of insulation design for pulsed power systems, the parameters of a layered composite system should be designed with careful consideration given to the applied impulse characteristics and material choice, if the desired performance is to be achieved.

## V. Application to Gas Insulated System Spacers

### A. Field at the Gas-Spacer Interface

As suggested in section I, one possible solution to allow for the continued miniaturization of various components in high voltage gas insulated equipment (e.g. gas insulated transmission lines (GIL)) relies on functionally graded solid dielectric spacers. Most importantly, the electric field distribution at the gas-spacer interface - particularly at the triple-junction formed between spacer, gas, and electrode - essentially dictates the breakdown strength of the system, due to the high level of field enhancement that can occur within this region. Graded spacers have been shown to successfully reduce the electric field enhancement factor at triple-junctions, which reduces the probability of electrical breakdown and subsequent system failure.

The model developed in this study does not explicitly consider the gas-spacer interface, however, this follow-on section shows that the field magnitude and distribution at the gas-spacer interface can be roughly approximated to a reasonable degree by the present analytical model, thereby providing a valuable design tool for the analysis of gas-insulated components under transient stress. One may consider a radially symmetric disk-type spacer employed in GIL. This spacer can be approximated using the concentric cylindrical geometry of section III-D and Fig. 2. This geometry is a simplification, particularly for some GILs used in power equipment, which consist of considerably more complex geometries. However, for spacers which are close to disk-like, e.g., as shown in [39], [40], or for small-scale non-standard systems used in some pulsed applications, which continue to employ simple disk-like geometries, they can be considered well-represented by the present model. Fig. 10 encloses the finite-element computed field distribution surrounding a simplified model of a disk-type spacer, with a radial dimension of $r_n - r_0$ = 5 cm, axial thickness of 3 cm, and with a conductor radius of $r_0$ = 2 cm. The 150 kV 1.2/50 $\mu$s lightning impulse described in Table I

was applied. Fig. 10(a) was generated with a homogeneous spacer material with identical properties in each layer of $(\varepsilon_r, \sigma)$ = (2.3, $10^{-14}$ S/m), contrasting that of Fig. 10(b), which was functionally graded following the 20-layer 'U'-shaped profile as before, for both relative permittivity and electrical conductivity. $E_{TJ}$ denotes the maximum field magnitude at both the spacer-gas-electrode triple-junctions.

The grading effect is evident in Fig. 10, with the net effect of the electric field being redistributed toward the middle of the spacer where permittivity and conductivity are at their lowest. As such, the field enhancement at the triple-junctions near the HV and ground electrodes were reduced. The maximum recorded value of $E_{TJ}$ with an ungraded spacer was ∼14 kV/mm at the anode and ∼6 kV/mm at the cathode, compared to respective values of ∼3 kV/mm and ∼1.3 kV/mm when the spacer was graded, corresponding to approximately 78% field reduction at both points. The field distribution at the gas-spacer interface (on the side of the gas) is shown in Fig. 11 (dashed line), which is compared to the analytically predicted field distribution modelled by (20) (solid line) in the spacer bulk. At any time, $t$, one may observe that the bulk field is a reasonable approximation of the field at the interface, particularly with regards to the shape of the redistributed field. While the analytical model does not provide exact field values at the interface, the general variation of the graded field is able to be approximated spatially and temporally. The model therefore provides a possible method for the rapid estimation of field redistribution at FGM-gas interfaces in GIS or other similar layered systems under time-varying stress, which may help to accelerate the design process of novel insulation technology. There are, of course, limitations to such an analytical approach. For example, the 2D polar approximation would likely become inaccurate as the thickness of the spacer decreases, since the derivation is limited by the assumption of invariance along the $z$ direction.

Despite this, the model has potential to be an important tool for the design of other pulsed power systems where the characteristics of the transient field is important, such as in PEF chambers. In these cases, the model may be used to estimate the transient field in an existing system; or be used to inform material choice to modulate the applied field with the aim to attain the optimal wave-shape for a specific application.

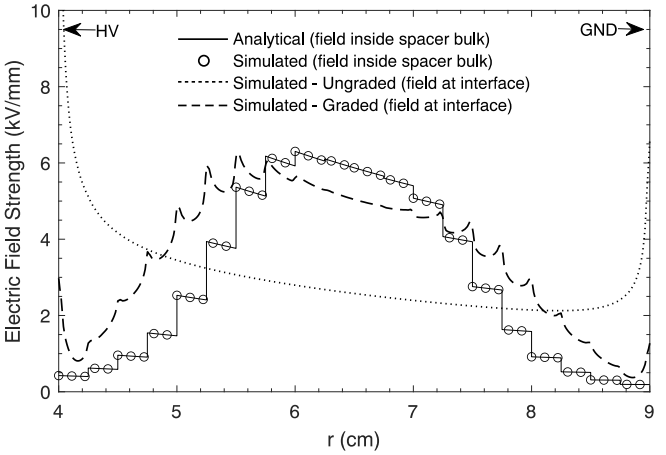


Fig. 11. The analytically predicted bulk field in the composite compared to the simulated field along the gas-spacer interface. Field measurement for the interface is taken along the dashed contour of Fig. 10 (on the side of the gas), while simulation results for the bulk are taken down the centerline of the spacer. Data was recorded at the time when the peak electric field magnitude was reached inside the domain (Dotted and dashed lines are therefore taken at different times, while the solid line is generated from (20) at the same time as the dashed line.

## VI. Conclusion

By employing an analytical approach to multilayered dielectric composites, this article has shown that mathematical solutions exist for $n$-layer composites in one-dimensional planar and cylindrical geometries with arbitrary permittivity, conductivity, and layer thicknesses. Closed-form solutions have been shown to exist for up to 5 layers, while procedures for the solution when $n > 5$ have additionally been outlined. As such, the electric field can be computed without the need for finite-element software, allowing parametric and optimization studies to be conducted rapidly. Using the developed model, the analysis of a 20-layer composite was conducted under the application of fast-rising impulsive voltages. The transient response of the electric field inside the composite has been shown to be governed by the complex interplay between system relaxation time constants and input signal characteristics. The model has further been applied to FGMs for GIS spacer design, demonstrating the ability for the model to reasonably approximate the redistribution of the electric field at the gas-spacer interface of a graded disk-type spacer under time-varying energization. Considering this, the model may be a valuable tool for the rapid estimation of field redistribution in layered dielectric systems, which may help to accelerate the design process of novel and non-standard pulsed power systems when used alongside existing, more complex, modelling methods.

In general, much remains to be investigated regarding the influence of individual dielectric relaxation times on the overall response of the composite. The present model provides a convenient method to explore a vast range of composite configurations and to rapidly characterize their behaviour, and due to its generality, its application is far from limited to FGMs or impulsive signals. The $s$-domain solutions may be modified for any arbitrary input waveform, and the composite thicknesses are also variable. With this flexibility in mind, the model may be of high interest to research in a number of other fields, including microbiological cell modelling, pulsed electric field treatment chamber design, multilayered capacitor design, insulation for more-electric aircraft, or for high energy density storage devices. However, there exist clear limitations to the present model, examples including the use of simple one-dimensional geometry, and the neglecting of $\sigma(T, E)$ dependence which may become important in high-field or long-term steady state applications. In future work, it would be of great interest to investigate the effects of nonuniform conductivity in combination with layered dielectric material in order to further assess the suitability of FGM usage in environments at elevated temperatures or fields. Future experimental work would also be a significant step forward, both for model

validation purposes and for advancing the techniques for the practical realization of multilayered composites.

## Acknowledgments

T. Wong was supported in part by the Engineering and Physical Science Research Council (EPSRC) under grant number EP/T517938/1. For the purpose of open access, the authors have applied a Creative Commons Attribution (CC BY) licence to any Author Accepted Manuscript version arising from this submission.

## References

[1] B. X. Du, Z. H. Wang, J. Li, H. C. Liang, and Z. H. Li, "Epoxy insulator with surface graded-permittivity by magnetron sputtering for gas-insulated line," *IEEE Trans. Dielectr. Electr. Insul.*, vol. 27, no. 1, pp. 197-205, Feb. 2020.

[2] J. Li, H. C. Liang, B. X. Du, and Z. H. Wang, "Surface functional graded spacer for compact HVDC gaseous insulated system," *IEEE Trans. Dielectr. Electr. Insul.*, vol. 26, no. 2, pp. 664-667, Apr. 2019.

[3] T. Christen, L. Donzel, and F. Greuter, "Nonlinear Resistive Electric Field Grading Part 1: Theory and Simulation," *IEEE Trans. Electr. Insul. Mag.*, vol. 26, no. 6, pp. 47-59, Dec. 2010.

[4] A. Can-Ortiz, L. Laudebat, Z. Valdez-Nava, and S. Diaham, "Nonlinear Electrical Conduction in Polymer Composites for Field Grading in High-Voltage Applications: A Review," *Polymers*, vol. 13, no. 9, pp. 1370, Apr. 2021.

[5] M. Pradhan, H. Greijer, G. Eriksson, and M. Unge, "Functional behaviours of electric field grading composite materials," *IEEE Trans. Dielectr. Electr. Insul.*, vol. 23, no. 2, pp. 768-778, Apr. 2016.

[6] X. Zhao *et al.*, "Grading of electric field distribution of AC polymeric outdoor insulators using field grading material," *IEEE Trans. Dielectr. Electr. Insul.*, vol. 26, no. 4, pp. 1253-1260, Aug. 2019.

[7] Rachmawati, H. Kojima, N. Hayakawa, K. Kato, and N. Zebouchi, "Electric Field Simulation of Permittivity and Conductivity Graded Materials ($\varepsilon/\sigma$-FGM) for HVDC GIS Spacers," *IEEE Trans. Dielectr. Electr. Insul.*, vol.28, no. 2, pp. 736-744, Apr. 2021.

[8] M. Kurimoto, H. Ozaki, T. Sawada, T. Funabashi, T. Kato, and Y. Suzuoki, "FEM Simulation of local field enhancement close to lamination interface of permittivity-graded material," *Electron. Commun. Jpn.*, Wiley, vol. 101, no. 6, pp. 48-57, Jun. 2018.

[9] N. Hayakawa, J. Ishiguro, H. Kojima, K. Kato, and H. Okubo, "Fabrication and simulation of permittivity graded materials for electric field grading of gas insulated power apparatus," *IEEE Trans. Dielectr. Electr. Insul.*, vol. 23, no. 1, pp. 547-554, Feb. 2016.

[10] X. Li *et al.*, "3D printing fabrication of conductivity non-uniform insulator for surface flashover mitigation," *IEEE Trans. Dielectr. Electr. Insul.*, vol. 26, no. 4, pp. 1172-1180, Aug. 2019.

[11] N. Hayakawa, Y. Miyaji, H. Kojima, and K. Kato, "Simulation on discharge inception voltage improvement of GIS spacer with permittivity graded materials ($\varepsilon$-FGM) using flexible mixture casting method," *IEEE Trans. Dielectr. Electr. Insul.*, vol. 26, no. 5, pp. 1218-1323, Aug. 2018.

[12] T. Imai, Y. Hoshina, K. Kojima, and N. Hayakawa, "Resin injection behavior in process of manufacturing insulation spacer with permittivity gradient using computational fluid dynamics," *IEEE Trans. Dielectr. Electr. Insul.*, vol. 26, no. 5, pp. 1669-1677, Oct. 2019.

[13] V. Boggarapu *et al.*, "State of the art in functionally graded materials," *Compos. Struct.*, vol. 262, pp. 113596, Apr. 2021.

[14] N. Hayashi, K. Kawahara, M. Sumikura, M. Hara, and F. Endo, "Electric field control by permittivity functionally graded materials and their lightning impulse withstand voltages for surface breakdown," *IEEE Intl. Symp. Electr. Insul.*, 2002.

[15] M. Kurimoto, K. Kato, M. Hanai, Y. Hoshina, M. Takei, and H. Okubo, "Application of functionally graded material for reducing electric field on electrode and spacer interface," *IEEE Trans. Dielectr. Electr. Insul.*, vol. 17, no 1, pp. 256-263, Feb. 2010.

[16] H. Ju, B. Kim, and K. Ko, "Optimal design of an elliptically graded permittivity spacer configuration in gas insulated switchgear," *IEEE Trans. Dielectr. Electr. Insul.*, vol. 18, no. 4, pp. 1268-1273, Aug. 2011.

[17] H. Ju, K. Ko, and D. Kim, "Optimization of a grounded electrode shape in gas insulated switchgear with a reversely elliptical permittivity graded insulator," *IEEE Trans. Dielectr. Electr. Insul.*, vol. 20, no. 5, pp. 1749-1754, Oct. 2013.

[18] N. Hayakawa, J. Shimomura, T. Nakano, M. Hanai, K. Kato, and H. Okubo, "Fabrication technique of permittivity graded materials (FGM) for disk-type solid insulator," *Annu. Rep. Conf. Electr. Insul. Dielectr. Phenom. (CEIDP)*, 2012.

[19] T. Imai, M. Takeuchi, Y. Hoshina, H. Kojima, and N. Hayakawa, "Comparison of permittivity gradient in resin injected and simulated cone-shaped spacers," *IEEE Trans. Dielectr. Electr. Insul.*, vol. 26, no. 5, pp. 1678-1685, Oct. 2019

[20] B. X. Du, Z. Y. Ran, J. Li, H. C. Liang, "Novel insulator with interfacial $\sigma$-FGM for DC compact gaseous insulated pipeline," *IEEE Trans. Dielectr. Electr. Insul.*, vol. 26, no. 3, pp. 818-825, May 2019.

[21] Y. Zhang *et al.*, "Optimal Design of Functionally Graded Power Cable Joint Utilizing Silicone Rubber/Carbon Nanotube Composites," *IEEE Access*, vol. 9, pp. 123689-123703, Aug. 2021.

[22] M. Talaat, A. El-Zein, and M. Amin, "Electric field simulation for uniform and FGM cone type spacer with adhering sperical conducting particle in GIS," *IEEE Trans. Dielectr. Electr. Insul.*, vol. 25, no. 1, pp. 339-351, Feb. 2018.

[23] J. Lehr, R. Pralhad, "Foundations of Pulsed Power Technology," *Wiley-IEEE Press*, 2018.

[24] A. R. Dick, S. J. MacGregor, M. T. Buttram, R. C. Pate, L. F. Rinehart, and K. R. Prestwich, "Breakdown phenomena in ultra-fast plasma closing switches," *IEEE Trans. Plasma Sci.*, vol. 28, no. 5, pp. 1456-1462, Oct. 2000.

[25] T. Kotnik, P. Kramar, G. Pucihar, D. Miklavcic, and M. Tarek, "Cell membrane electroporation - Part 1: The phenomenon," *IEEE Electr. Insul. Mag.*, vol. 28, no. 5, pp. 14-23, Aug. 2012.

[26] S. Min, G. A. Evrendilek, and H. Q. Zhang, "Pulsed Electric Fields Processing System, Microbial and Enzyme Inhibition, and Shelf Life Extension of Foods," *IEEE Trans. Plasma Sci.*, vol. 35, no. 1, pp. 59-73, Feb. 2007.

[27] A. C. Mermigkas, I. V. Timoshkin, S. J. MacGregor, M. J. Given, M. P. Wilson, and T. Wang, "Removal of Fine and Ultrafine Particles From Air by Microelectrostatic Precipitation," *IEEE Trans. Plasma Sci.*, vol. 41, no. 10, pp. 2842-2850, Apr. 2013.

[28] A. Sitzman, D. Suris, and J. Mallick, "Design, Construction, and Testing of an Inductive Pulsed-Power Supply for a Small Railgun," *IEEE Trans. Magn.*, vol. 43, no. 1, pp. 270-274, Dec. 2006.

[29] V. Adamec and J. H. Calderwood, "Electric-field-enhanced conductivity in dielectrics," *J. Phys. D: Appl. Phys.*, vol. 10, no. 6, Feb. 1977.

[30] J. H. Simpson, "The Time Delay in Conduction and Breakdown Processes in Amorphous Solids," *Proc. Phys. Soc. A*, vol. 63, no. 86, 1950.

[31] G. Eriksson, H. Greijer, M. Pradhan, and M. Unge, "Stress dependent conductivity of field grading materials under time-varying electrical fields," *Ann. Report Conf. Electr. Insul. Dielectr. Phenom.*, Montreal, QC, Canada, Oct. 2012.

[32] N. H. Abel, "Mémoire sur les équations algébriques, ou l'on démontre l'impossibilité de la resolution de l'équation générale du cinquiéme degrém" *Oeuvres Complétes de Niels Henrik Abel* (in French), Grøndahl & Søn, pp. 28-33, 1824.

[33] QuickField Professional version 6.4, Tera Analysis.

[34] Y. Zhou, S. Peng, J. Hu, and J. He, "Polymeric insulation materials for HVDC cables: Development, challenges, and future perspective," *IEEE Trans. Dielectr. Electr. Insul.*, vol. 24, no. 3, pp. 1308-1318, Jun. 2017.

[35] MACOR Machinable Glass Ceramic Data Sheet, Corning Inc. [Online]. Available: https://www.corning.com/worldwide/en/products/advanced-optics/product-materials/specialty-glass-and-glass-ceramics/glass-ceramics/macor.html

[36] M. Halloum, B. Reddy, and G. Reddy, "Stress Control of Polymeric Outdoor Insulators Using Nonlinear Resistive Field Grading Materials Operating Under Different Conditions," *IEEE Trans. Dielectr. Electr. Insul.*, vol. 29, no. 3, pp. 1175-1182, Jun. 2022.

[37] A. Naeini, E. A. Cherney, and S. H. Jayaram, "Effect of conductivity on the thermal and electrical properties of the stress grading system of an inverter-fed rotating machine," *IEEE Trans. Dielectr. Electr. Insul.*, vol. 26, no. 1, pp. 179-186, Feb. 2019.

[38] High-voltage test techniques, IEC Standard 60060, 2010.

[39] A. H. Cookson, "Review of high-voltage gas breakdown and insulators in compressed gas," *IEE Proc. A. (Phys. Sci., Measurement, Management and Education, Reviews*, vol. 128, no. 4, pp. 303-312, May 1981.

[40] N. Zebouchi and M. A. Haddad, "A Review on Real-Size Epoxy Cast Resin Insulators for Compact High Voltage Direct Current Gas Insulated Switchgears (GIS) and Gas Insulated Transmission Lines (GIL) - Current Achievements and Envisaged Research and Development," *Energies*, vol. 13, no. 23, Dec. 2020.

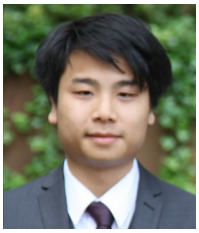

**Timothy Wong** received the B.Eng. and M.Eng. degrees in electrical and mechanical engineering with international study from The University of Strathclyde, Glasgow, U.K., in 2020 and 2021, respectively. He is currently pursuing the degree of Ph.D. in electronic and electrical engineering at the University of Strathclyde, Glasgow, U.K., with the High Voltage Technologies research group. His current research include the pulsed breakdown of solid-solid dielectric interfaces, solid-gas interfaces, computational modelling of fast ionisation fronts and streamer discharges in gas and gas-solid topologies, and pulsed power insulation systems. He was the recipient of the IMechE student award in 2020 and is currently a graduate student member of the Dielectrics and Electrical Insulation society (DEIS) and the Nuclear and Plasma Sciences society (NPSS).

**Igor Timoshkin** received the degree in physics from Moscow State University, Moscow, Russia, in 1992, and the Ph.D. degree from the Imperial College of Science, Technology, and Medicine (ICSTM), London, U.K., in 2001. He was a researcher at Moscow State Agro-Engineering University, Moscow, and then at the Institute for High Temperatures of Russian Academy of Sciences, Moscow. In 1997 he joined ICSTM. Then he joined the department of Electronic and Electrical Engineering, University of Strathclyde, Glasgow, U.K., in 2001, where he became a Reader in 2016. His research interests include dielectric materials, pulsed power, transient spark discharges, environmental applications of non-thermal plasma discharges. Dr. Timoshkin is a Voting Member of the Pulsed Power Science and Technology Committee in the IEEE Nuclear and Plasma Science Society; a member of International Advisory Committee of the IEEE Conference on Dielectric Liquids, a member of the International Scientific Committee of the Gas Discharges and Their Applications Conference, and a Subject Editor of IET Nanodielectrics.

**Scott MacGregor** received the B.Sc. and Ph.D. degrees from the University of Strathclyde, Glasgow, U.K., in 1982 and 1986, respectively. He was a Pulsed-Power Research Fellow in 1986 and a Lecturer in pulsed-power technology in 1989. In 1994, he became a Senior Lecturer, with a promotion to Reader and a Professor of High Voltage Engineering, in 1999 and 2001, respectively. In 2006 and 2010, he became the Head of the Department of Electronic and Electrical Engineering and the Executive Dean of the Faculty of Engineering, and has been the Vice-Principal with the University of Strathclyde, since 2014. His current research interests include high-voltage pulse generation, high-frequency diagnostics, high-power repetitive switching, high-speed switching, electronic methods for food pasteurization and sterilization, the generation of high-power ultrasound (HPU), plasma channel drilling, pulsed-plasma cleaning of pipes, and the stimulation of oil wells with HPU. Prof. MacGregor was a recipient of the 2013 IEEE Peter Haas Award. He was an Associated Editor of the IEEE Transactions of Dielectrics and Electrical Insulation in 2015.

**Mark Wilson** was born in Stranraer, Scotland, in 1982. He received the B.Eng. (with honours), M.Phil., and Ph.D. degrees in electronic and electrical engineering from the University of Strathclyde, Glasgow, U.K., in 2004, 2007, and 2011, respectively. He is presently based in the High Voltage Technologies research group at the University of Strathclyde, where his research interests include interfacial surface flashover, nanodielectrics, and the practical applications of high-power ultrasound, corona discharges, and pulsed electric fields. Mark is a member of the IEEE Nuclear and Plasma Science Society, from whom he received a Graduate Scholarship Award in 2011, the IEEE Dielectrics and Electrical Insulation Society, and the IET.

**Martin Given** received the B.Sc. degree in physics from the University of Sussex, Brighton, U.K., in 1981, and the Ph.D. degree in electronic and electrical engineering from the University of Strathclyde, Glasgow, U.K., in 1996. He is currently a Senior Lecturer with the Department of Electronic and Electrical Engineering, University of Strathclyde. His current research interests include ageing processes and condition monitoring in solid and liquid insulation systems, high-speed switching, and pulsed power.